Electronic Supplementary Material (ESI) for Journal of Materials Chemistry A.

pH Dependent Photocatalytic Hydrogen Evolution by Self-Assembled Perylene Bisimides

Michael C. Nolan[a,b,c], James J. Walsh[c,d], Laura L. E. Mears[b,c], Emily R. Draper[a,b], Matthew Wallace[b], Michael Barrow[b], Bart Dietrich[a,b], Stephen M. King[e], Alexander J. Cowan[c]* and Dave J. Adams[a,b]*

Supporting Information

[a.] *School of Chemistry, University of Glasgow, Glasgow, G12 8QQ, U.K. Email: dave.adams@glasgow.ac.uk
[b.] Department of Chemistry, University of Liverpool, Crown Street, Liverpool L69 7ZD, U.K.
[c.] *Stephenson Institute for Renewable Energy, University of Liverpool, Chadwick Building, Peach Street, Liverpool L69 7ZF, U.K. Email: a.j.cowan@liverpool.ac.uk
[d.] School of Chemical Sciences, Dublin City University, Glasnevin, Dublin 9, Ireland.
[e.] STFC Pulsed Neutron and Muon Source, Science and Technology Facilities Council, Rutherford Appleton Laboratory, Harwell Campus, Didcot, OX11 0QX, U.K.

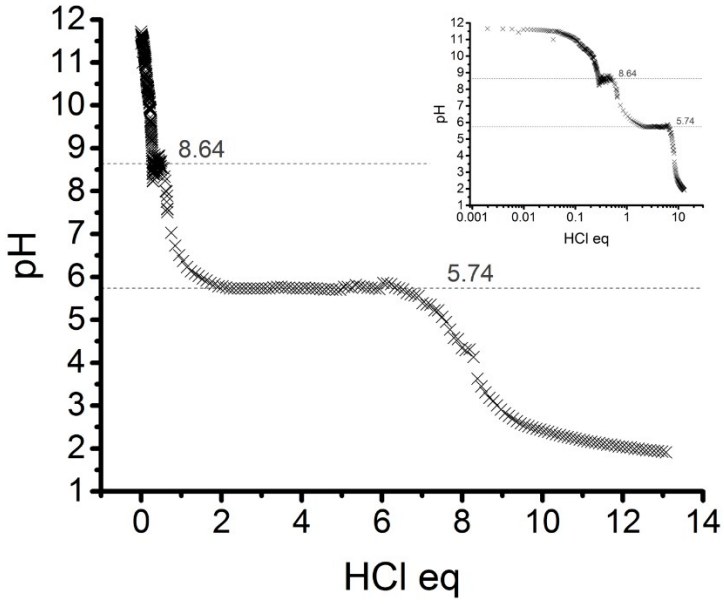

Figure S1. pK_a titration of PBI-F solution (10 mg/mL) starting from 2 molar equivalents of $NaOH_{(aq)}$ at pH 12 and decreasing the pH using 10 µL aliquots of 0.1M $HCl_{(aq)}$. Horizontal lines indicate the two apparent pK_a buffering regions. (inset) HCl eq. plotted on a log scale to reveal the first apparent pK_a in more detail.

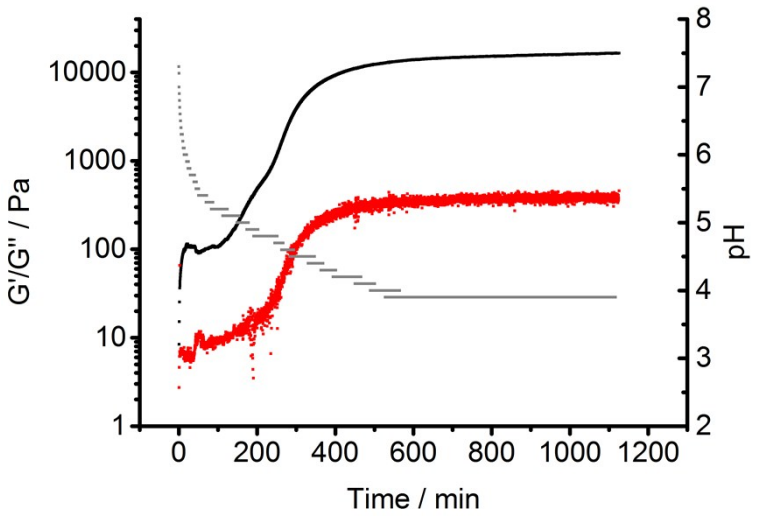

Figure S2. Time sweep for gelation using 8 mg/mL GdL in a PBI-F solution (10 mg/mL) containing 2 molar equivalents $NaOH_{(aq)}$. Grey lines indicate pH (right y-axis) of the gel. Data points indicate G' (black) and G'' (red) during the evolution of the PBI-F gel over time at a constant frequency. Rheology was performed at 0.5 % strain and 10 rad/s at 25 °C.

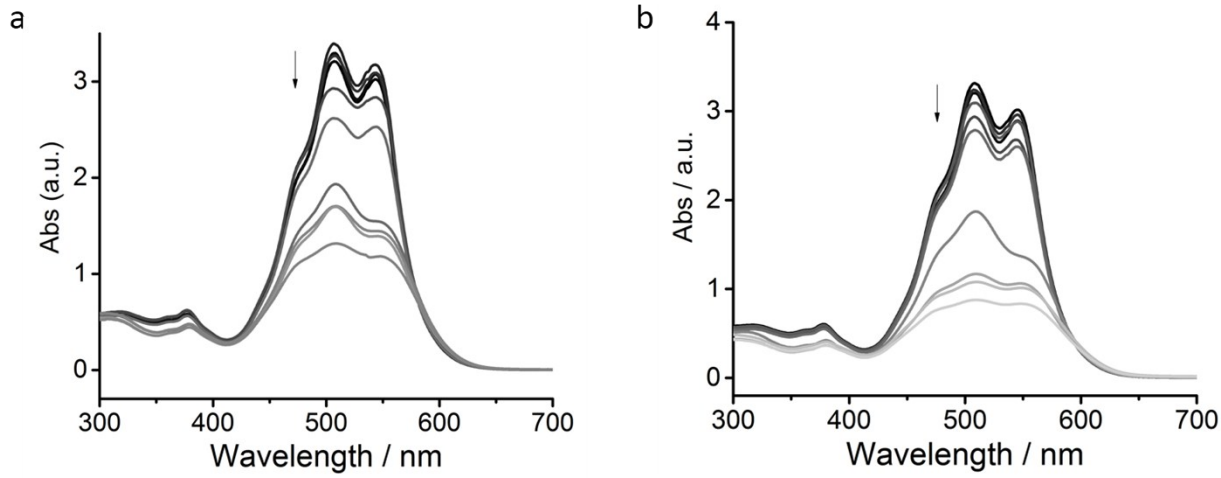

Figure S3. UV-Vis absorption spectra of PBI-F solutions (10 mg/mL) in (a) 20% v/v % methanol$_{(aq)}$ and (b) in H_2O. Arrows indicate the decrease in pH as listed: pH 11, 10, 9, 8, 7, 6, 5, 4, 3, 2.

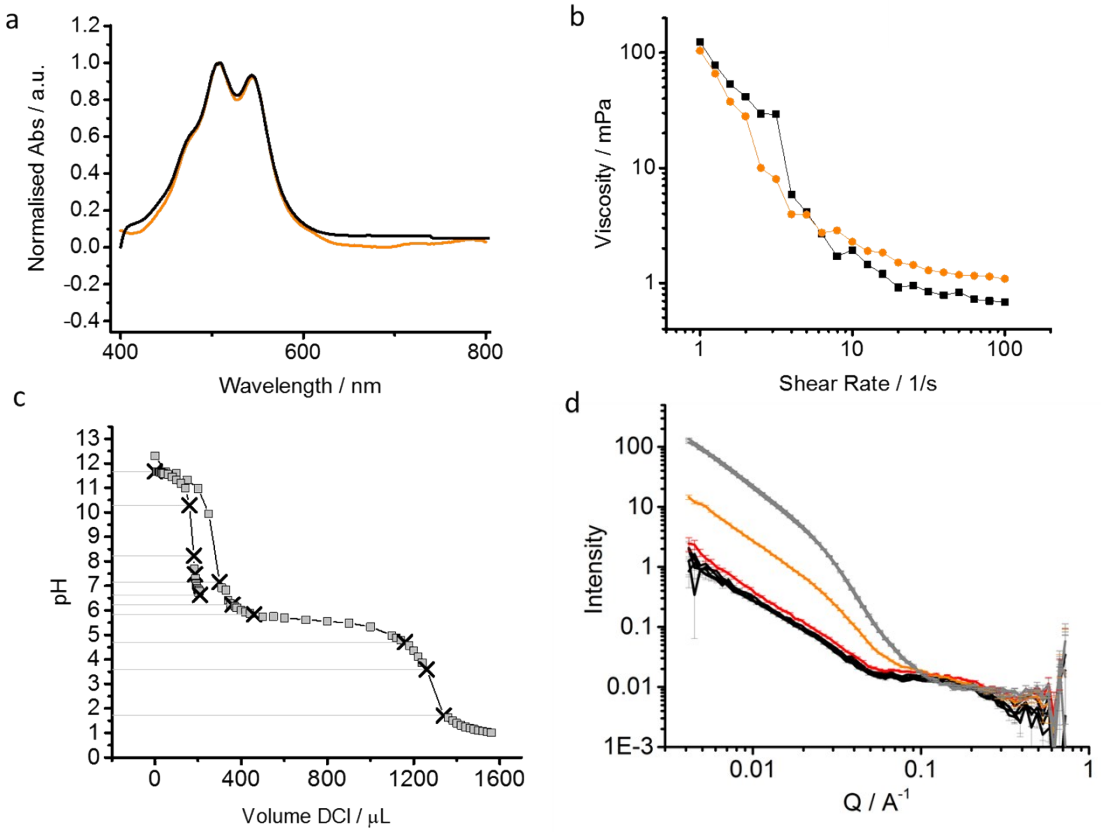

Figure S4. (a) UV-Vis absorbance spectra of PBI-F in 20 v/v % methanol$_{(aq)}$ (black) and deuterated solvents (orange); (b) Viscosity measurements; (c) pH drop, converted from pD,[1] of two stock solutions where crosses indicate where 1 mL aliquots were removed from the starting 20 mL solution for SANS measurements; (d) SANS data collected in a 5 mm pathlength quartz cuvette. pH 11.67, 10.29, 8.40, 7.42, 7.16 (black); pH 6.63 (red); pH 5.84 (orange) and pH 4.64, 3.52, 1.9 (grey).

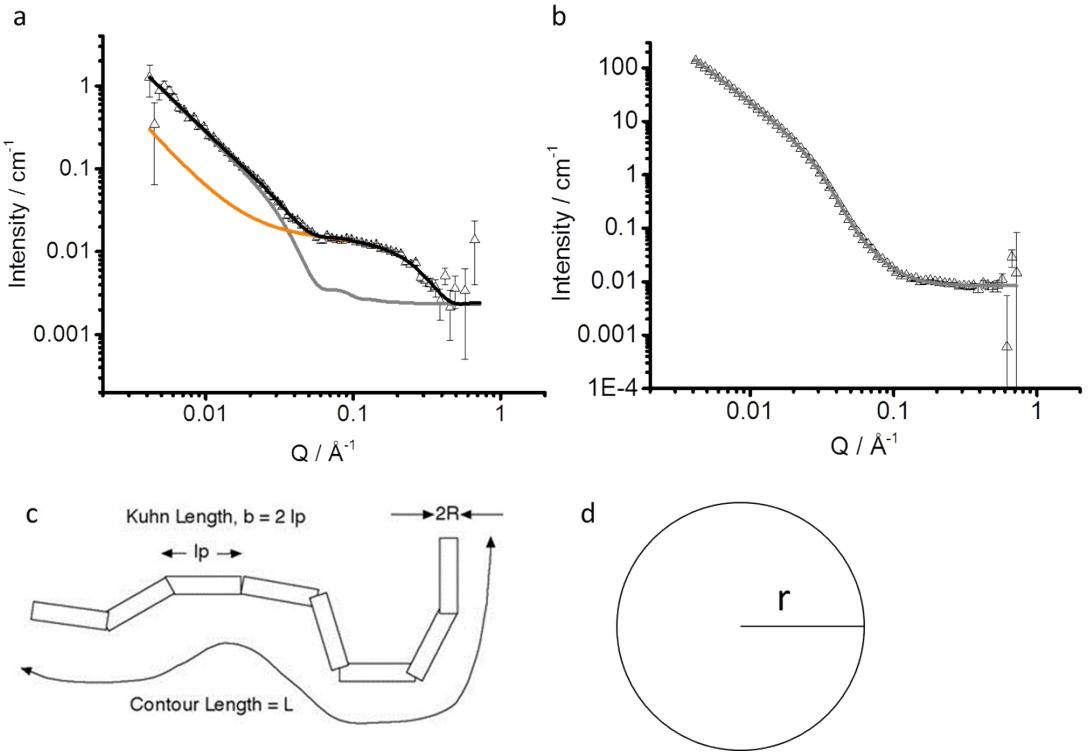

Figure S5. (a) SANS from PBI-F solution at pH 10.6 with fitting lines showing contribution of a flexible cylinder model (grey) and a spherical model (orange) to attain a complete fit (black) of the raw data (triangles with error bars) (b) scattering data from a pH 3.5 solution showing a complete fit to the flexible cylinder model. All models also include a Q^{-m} power law. Schematic representations of (c) the flexible cylinder and (d) sphere.

A composite model was formed from the addition of the absolute power law (PL), flexible cylinder (FC) and sphere (Sp) models available in SasView (Equation 1).[2] Constant scattering length density (SLD) parameters were used: 6.26 x 10^{-6} Å^{-2} for the MeOD/D_2O solvent, 2.17 x 10^{-6} Å^{-2} for the flexible cylinder and sphere.

$$I = SF_O\{SF_{PL}.P(Q)_{PL} + SF_{FC}.P(Q)_{FC} + SF_{Sp}.P(Q)_{Sp}\} + Background \quad (1)$$

where P(Q) is the relevant scattering form factor and SF is the relevant scale factor and SF_o is the over scale, which was fixed at 1 during fitting.

Uncertainties were determined by where the model deviated from a visibly good fit. For the longest lengths only a lower limit can be accurately determined as they move beyond the measurement limits of the instrument.

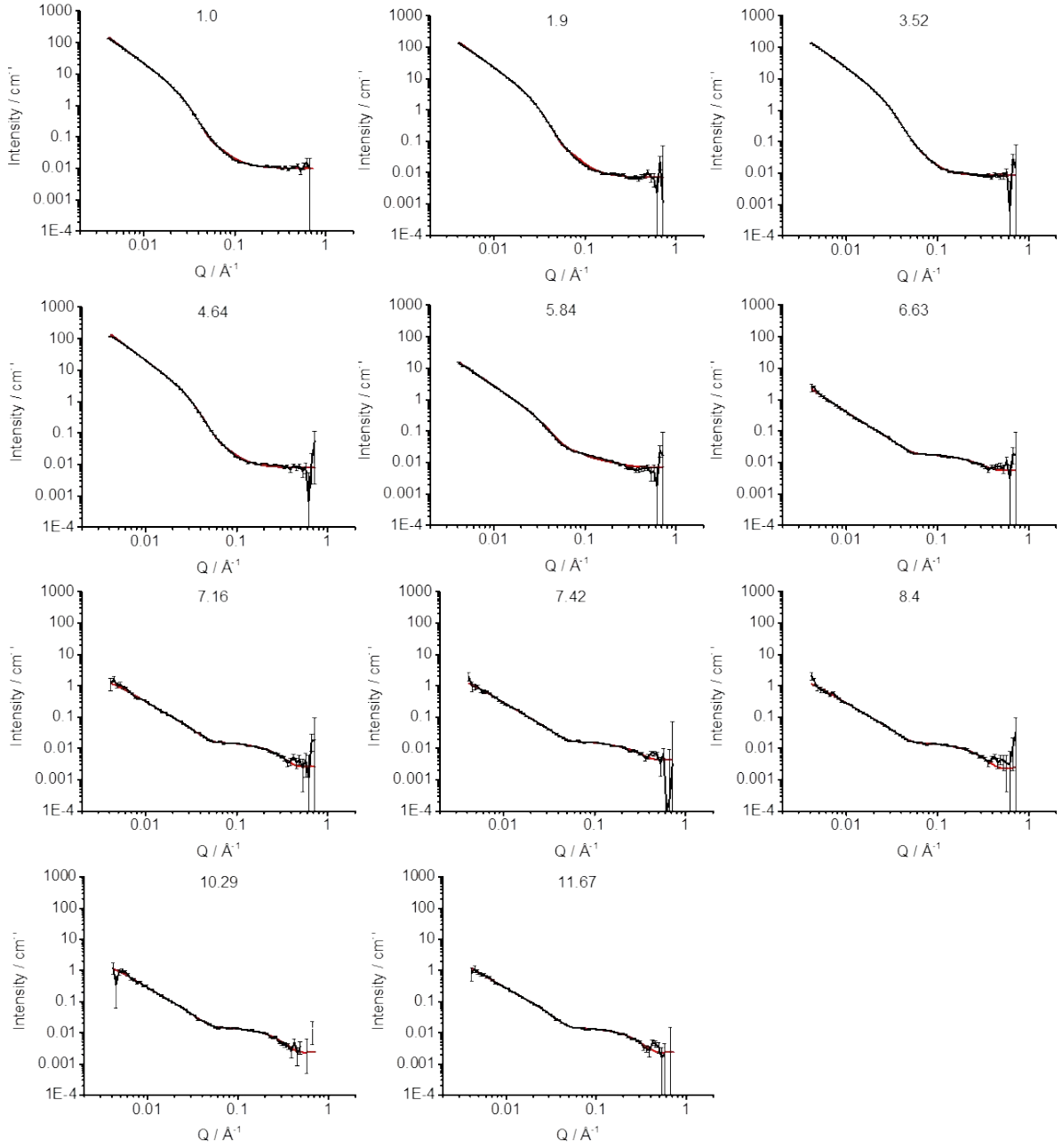

Figure S6. SANS data (black symbols) with model-fitted curves (red lines) of PBI-F (10 mg/mL) in D_2O with 20 v/v % deuterated methanol$_{(aq)}$ at different pD values.

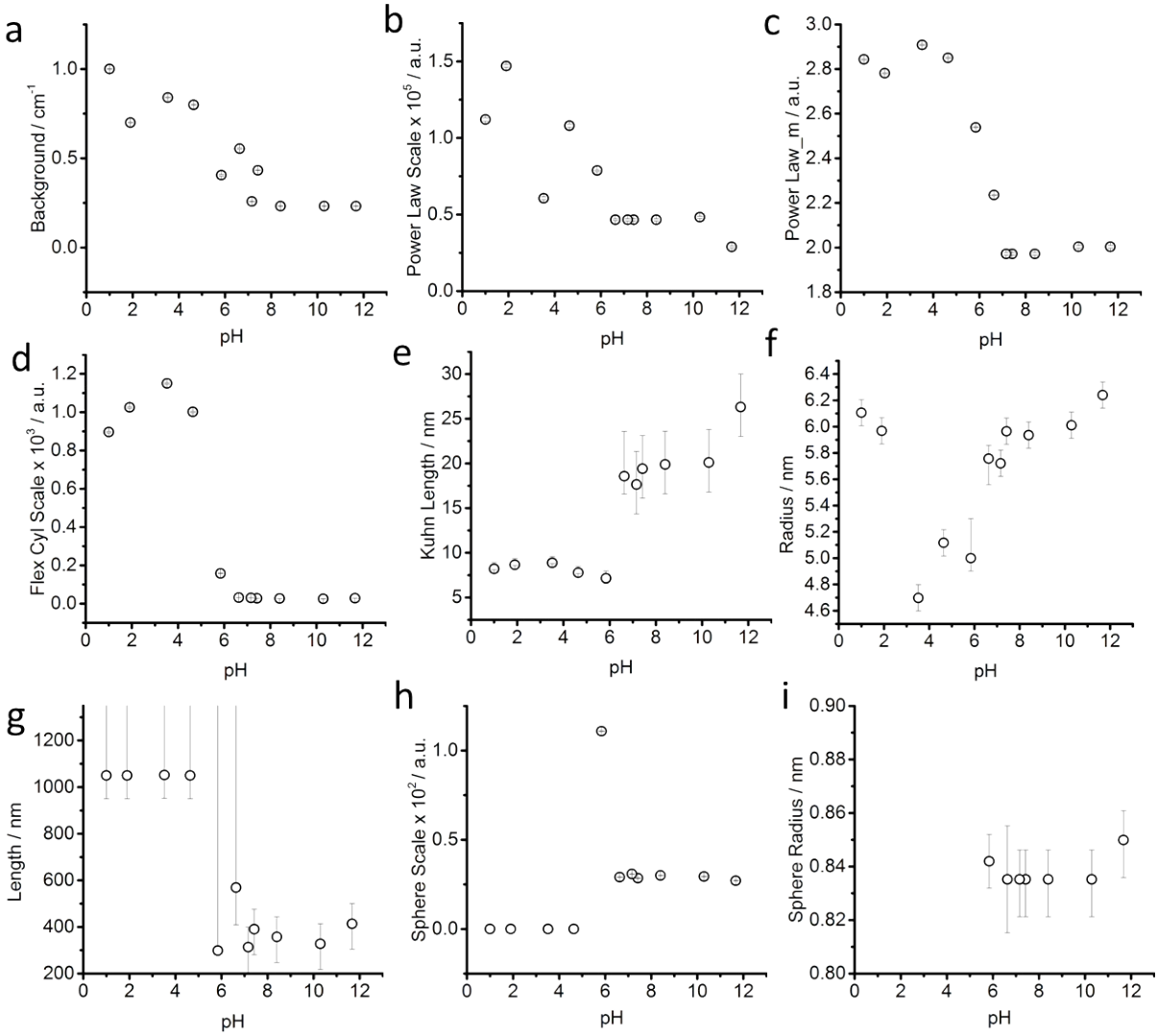

Figure S7. Fitted parameters for the curves shown in Figure S6. (a) background; (b) power law model scale; (c) power law exponent 'm'; (d) flexible cylinder model scale; (e) flexible cylinder Kuhn length; (f) flexible cylinder radii; (g) flexible cylinder length; (h) sphere model scale and (g) sphere radii. Lower and upper uncertainties with the parameters have been investigated and plotted as error bars. Error bars are shown for all points and are sometimes smaller than the scatter circle.

Diffusion NMR

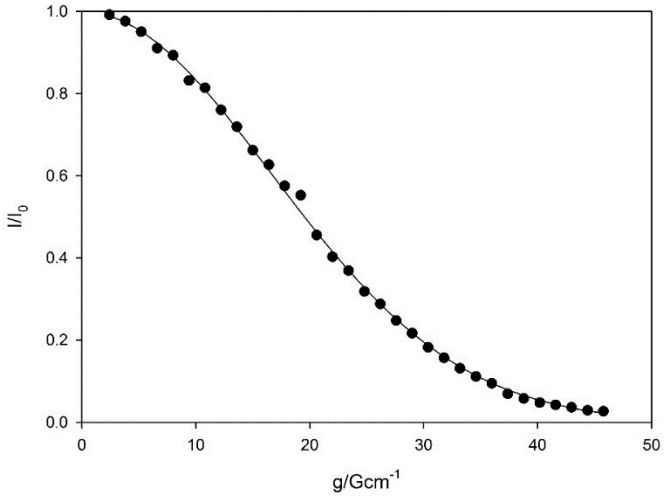

Figure S8. PFG-NMR attenuation plot for PBI-F in 20% MeOH, 80% H_2O at pH 11.2. The solid line is a best fit to Equation 2.

Diffusion NMR (PFG-NMR) experiments were performed using a modified double stimulated echo sequence based on that of Jerschow and Muller[3] (Bruker pulse program library dstegp3s). The sequence was modified to include pre-saturation of the methanol resonance during the relaxation delay (5 s) and a double-echo WATERGATE sequence of Liu *et al.*[4] (Bruker pulse program library ZGGPW5) after the PFG-NMR sequence to supress the H_2O resonance. Spectra were recorded as a function of the gradient amplitude, g, in 32 steps and 16 scans from 2.4 to 45.6 G/cm. The diffusion delay, Δ, was set at 0.2 s while the gradient pulse length, δ, was set at 2.9 ms. The delay between successive hard pulses in the selective WATERGATE train was set at 250 μs, corresponding to a 4000 Hz separation between the null points. The sample was maintained at a constant temperature of 298±0.5 K, the deviation in temperature during the experiment being less than 0.1 K. The aromatic resonances of PBI-F (7-8 ppm) were integrated and fitted to Equation 2 to obtain the diffusion coefficient, D:

$$\frac{I}{I_0} = exp\left[-\gamma^2 g^2 \delta^2 D\left(\Delta - \frac{\delta}{3} - \tau\right)\right] \qquad (2)$$

where: I and I_0 are integrals with and without an applied gradient, γ is the gyromagnetic ratio of ^1H and τ is a short delay during the pulse sequence (200 μs). From this, D was obtained as (1.55±0.02) x 10^{-10} m^2s^{-1} (uncertainty obtained using method of Brown et al.[5]). Applying the Einstein-Stokes equation (Equation 3)

$$R_h = \frac{k_B T}{6\pi\eta D} \qquad (3)$$

where k_B is Boltzmann's constant and T is the absolute temperature. , and using a viscosity (η) of 0.821 mPa.s,[6] we obtain a hydrodynamic radius (R_h) for the diffusing entities of 1.72±0.03 nm:

Quantification of amount of PBI-F visible by NMR

A 10 mg/mL solution of PBI-F was prepared in 80 % D_2O, 20% CD_3OD at a pD 10.4. The CH_2 resonances of the phenylalanine residues were integrated against the resonance of a 30 mM solution of TSP (3-(trimethylsilyl)-propionic-2,2-3,3-d_4 acid sodium salt) in an internal glass capillary. The integrals corresponded to 92% of a theoretical 10 mg/mL solution of PBI-F. The spectrum was acquired using a 30° flip angle, an acquisition time of 4 s and a relaxation delay of 20 s. 32 scans were recorded.

NOE and relaxation experiments to study aggregation of PBI-F

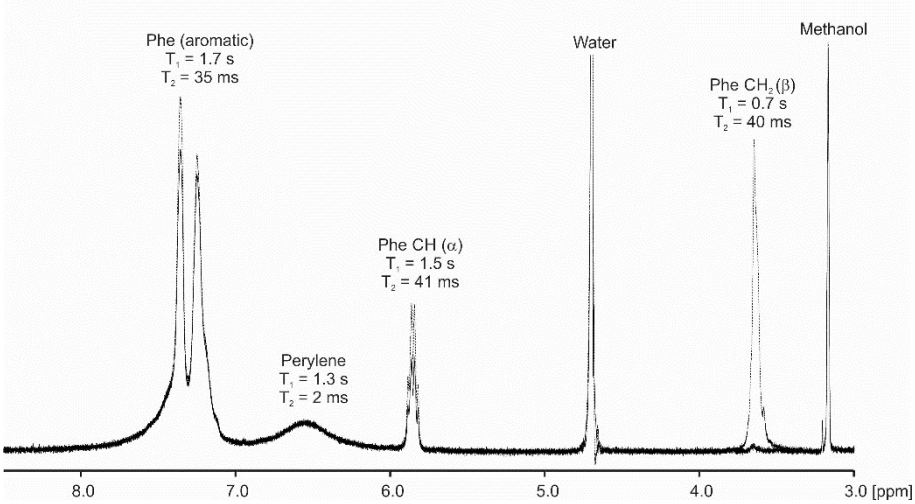

Figure S9. ^{1}H-NMR spectrum of a 10 mg/mL solution of PBI-F in 80 % D_2O, 20% CD_3OD with (solid) and without (dashed) pre-saturation applied to the CH_2 resonances of the phenylalanine (Phe) residues. ^{1}H T_1 and T_2 relaxation times are also indicated.

The CH_2 resonances of the phenylalanine residues were irradiated for 8 s using a train of 157 Gaussian pulses, each 50 ms in duration with a peak power of 24 Hz, followed by a 30^{o} hard pulse and signal acquisition (4 s). 8 scans were acquired. The other resonances of the phenylalanine residues are attenuated (negative NOE). The resonances are also much broader and display reduced T_1 and T_2 relaxation times compared to what would be expected for a freely-dissolved molecule of similar size. These results are all consistent with the NMR-visible PBI-F being in exchange with large aggregates.[7,8] T_1 and T_2 relaxation times were measured using the inversion-recovery and CPMG sequences respectively. For T_1, the signal intensity was acquired using sixteen delay values from 1 ms to 20 s. For T_2, the spacing between the π pulses was kept fixed at 2 ms and the number of pulses varied from 2 to 180 in sixteen steps.

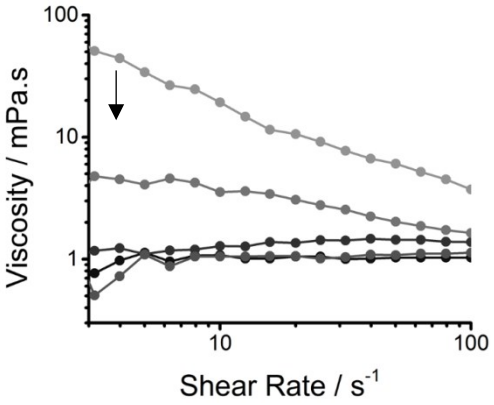

Figure S10. Viscosity of PBI-F (10 mg/mL) solutions in H_2O with 20 v/v% methanol. Viscosity decreasing as the pH is increased; pH 6.41, 7.68, 8.71, 9.42, 10.1.

Scanning Electron Microscopy (SEM)

Samples were prepared for SEM by placing a small amount of material onto a glass cover slip. The samples were allowed to fully dry for 24 hours in air. The glass slip was then attached to a 15 mm aluminium screw-in stub by a carbon tab. Samples were then measured in deceleration mode at 2 kV at a height of 3 mm using a Hitachi S4800 SEM.

Transmission Electron Microscopy (TEM)

Samples were prepared for TEM by pipetting a small amount of material onto a grid coated with a thin formvar film with a 200 mesh thick grid of Cu. The sample was left on the grid for 20 seconds and then lightly blotted from the side onto a filter paper to remove any excess solution. The grid was then imaged using a FEI 120kV Tecnai G2 Spirit BioTWIN TEM using a 120 kV accelerating voltage.

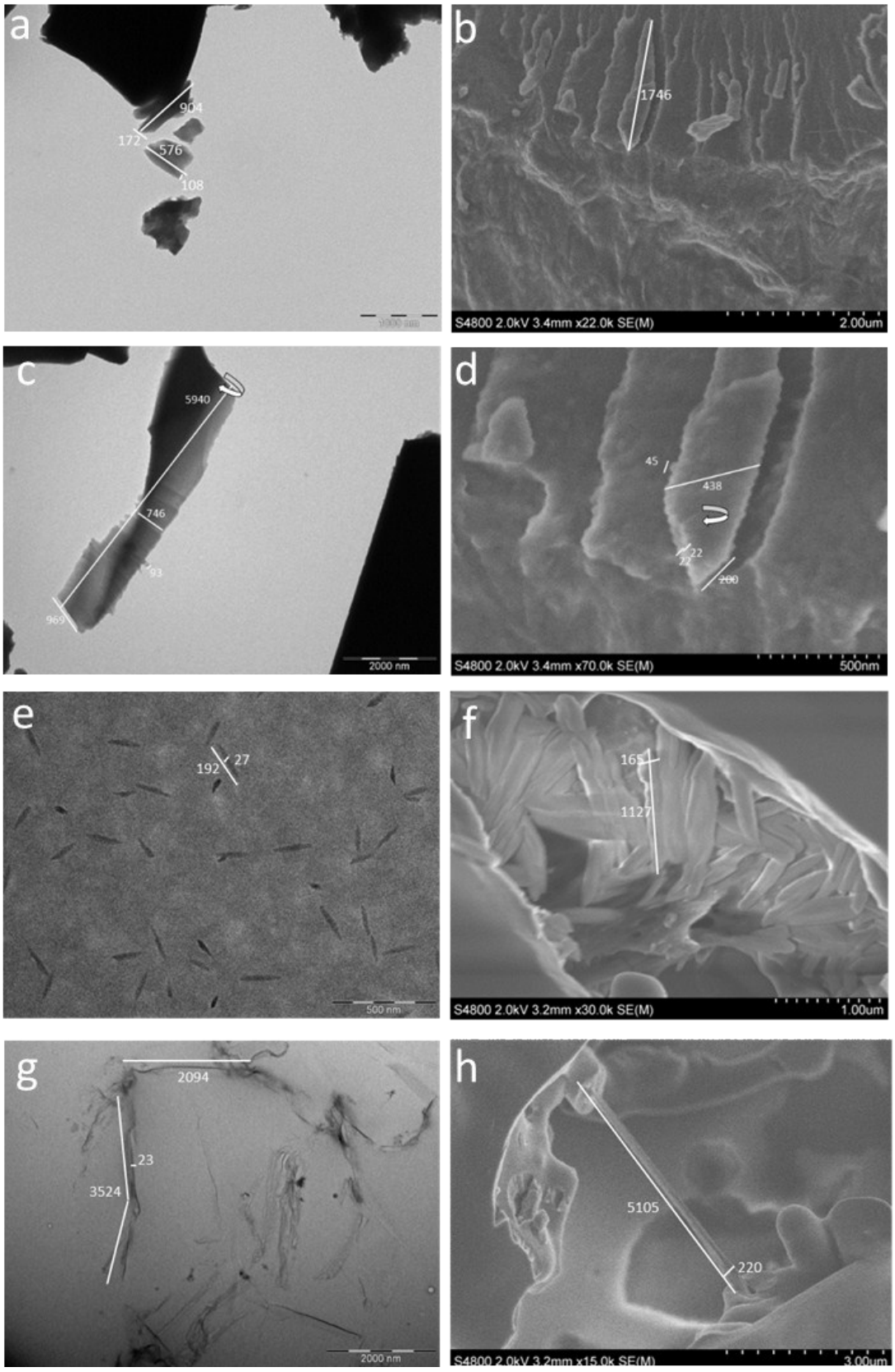

Figure S11. (a-d) images of dried aggregates collected from a pH 4.5 solution of PBI-F (10 mg/mL) in 20 v/v% methanol$_{(aq)}$, TEM (a, c) and SEM (b, d); (e-h) images of dried pH 10.5 solutions of PBI-F (10 mg/mL) in 20 v/v% methanol$_{(aq)}$, TEM (e, g) and SEM (f, h). Scale bars inset are: (a) 1000 nm; (b) 2000 nm; (c) 2000 nm (d) 500 nm; (e) 500 nm; (f) 1000 nm; (g) 2000 nm; (h) 3000 nm.

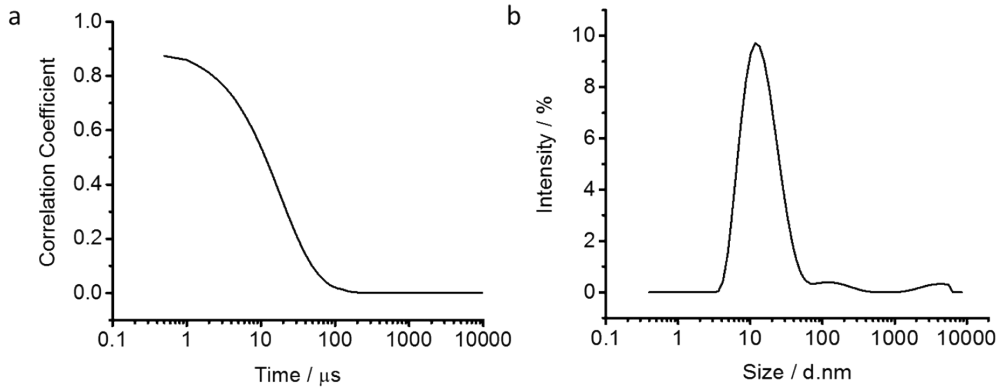

Figure S12. DLS data of PVP-Pt NPs. (a) Correlogram showing the correlation function where the y-axis is the normalised correlation function and (b) Size distribution by intensity. Three runs, each with 15 scans, were averaged for the final profile.

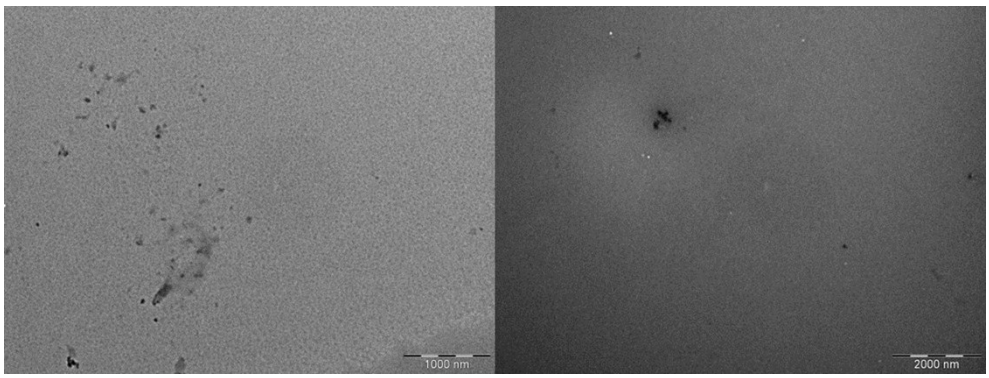

Figure S13. TEM images of PVP-Pt NPs. Samples were dabbed onto a grid and blotted to remove excess water. An accelerating voltage of 120 kV was used. The grids used had a 400 nm mesh copper grid with a carbon formvar coating. Scale bars inset are 1000 nm (left) and 2000 nm (right).

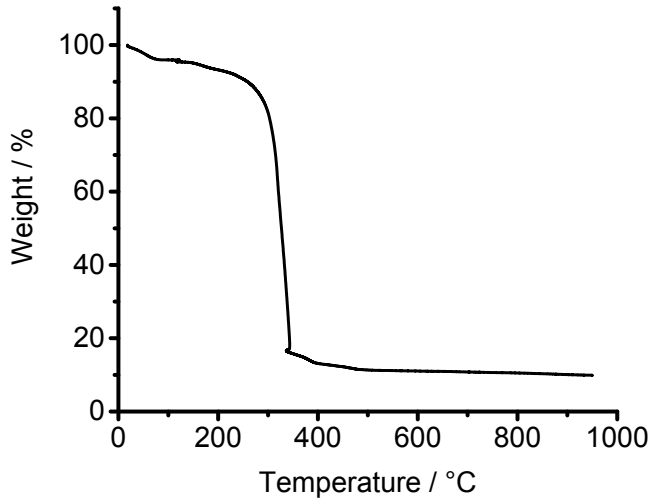

Figure S14. TGA of PVP-Pt NPs. Measurements were carried out on a TA Instruments SDT Q600 TGA machine using a constant air flow of 50 mL/min. Samples were heated up to 120 °C at a heating rate of 20 °C/min and kept at 120 °C for 20 minutes to remove any water, then ramped up to 1000 °C at a heating rate of 10 °C/min.

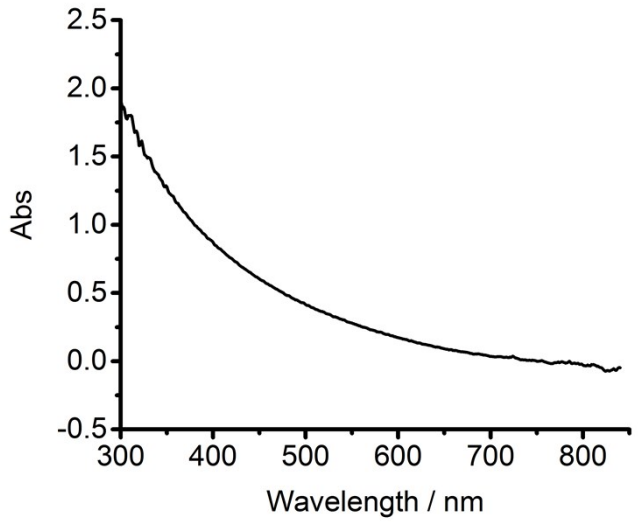

Figure S15. UV-Vis of PVP-Pt NPs. The UV-Vis spectrum was recorded in a quartz cuvette with a 1 cm path length with a Thermo Scientific NanoDrop UV-Vis spectrometer.

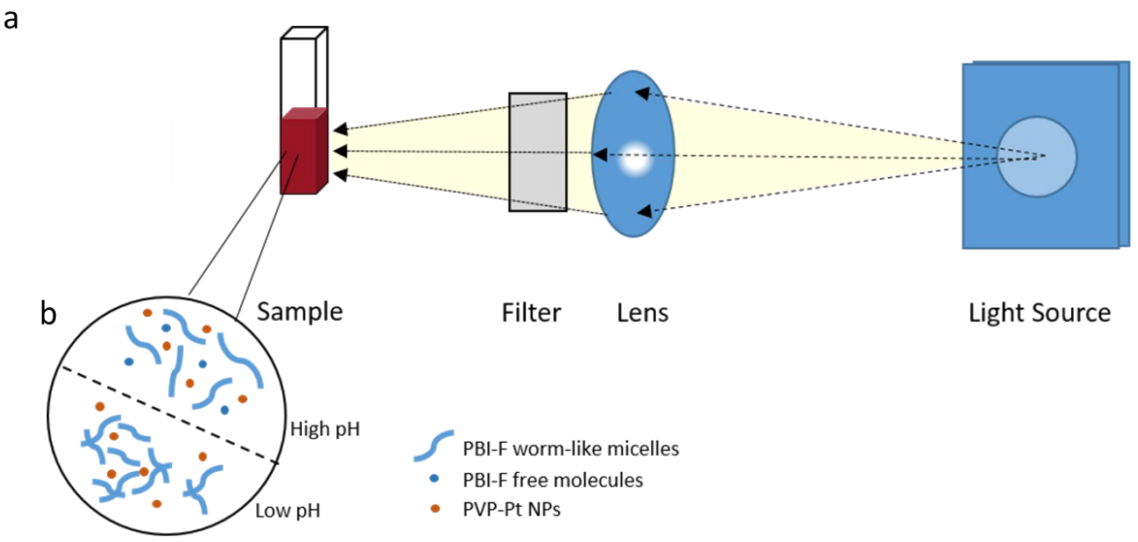

Figure S16. (a) Schematic of the setup used for photocatalytic hydrogen evolution experiments (b) Schematic of the PBI-F fibres, free PBI-F molecules and PVP-Pt NPs in solution at high and low pH. Interactions between PVP-Pt nanoparticles and PBI fibres are not known.

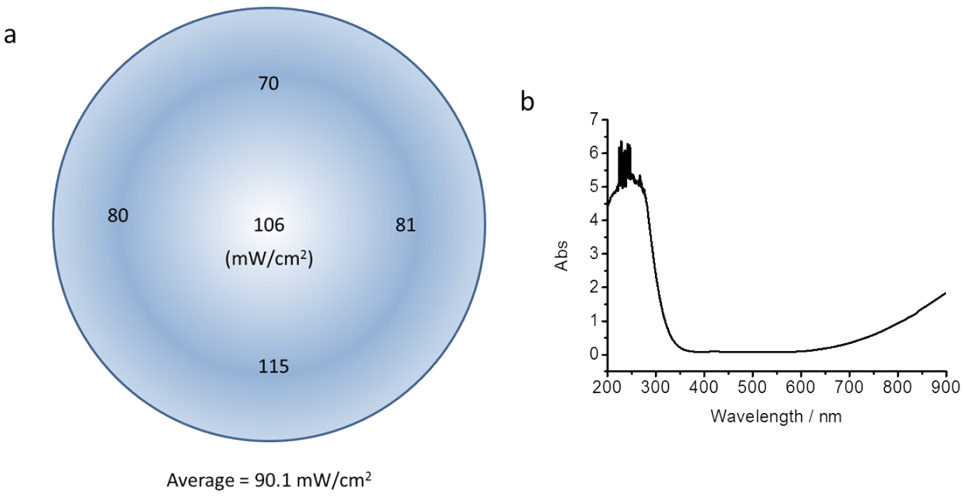

Figure S17. (a) Spectral power distribution of the light beam used to irradiate the sample. (b) The UV-Vis absorption spectrum of the demountable KG1 filter used.

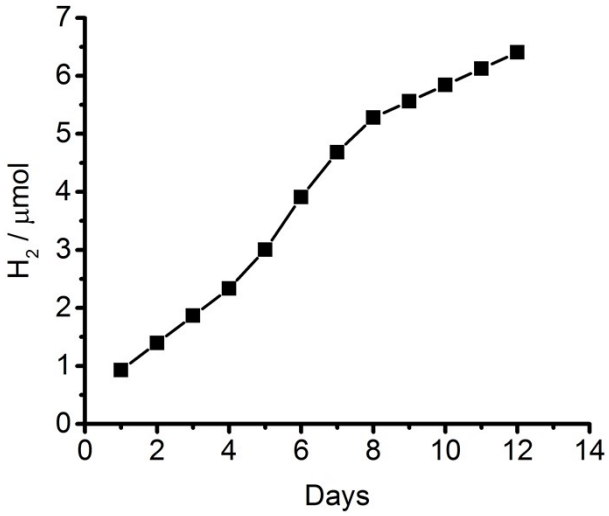

Figure S18. Photocatalytic hydrogen evolution over time of PBI-F/PVP-Pt NPs/20 v/v% methanol$_{(aq)}$ solution at pH 4.5. Each day the septum was replaced and the solution was re-purged for 20 minutes with argon.

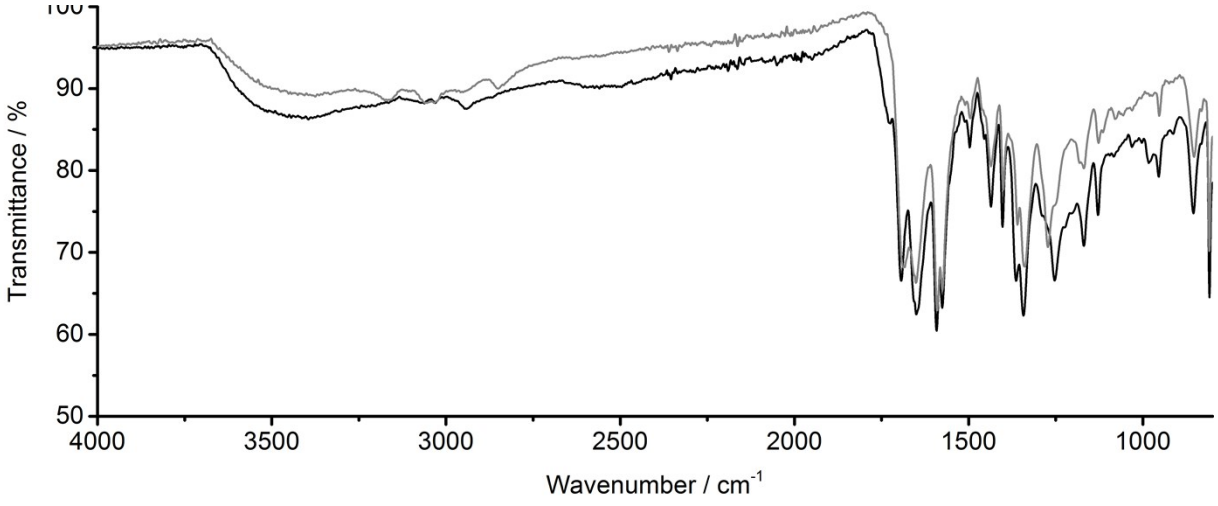

Figure S19. FTIR spectra of freeze-dried photocatalytic solutions (PBI-F/PVP-Pt NPs/20 v/v% methanol$_{(aq)}$) before (red) and after (black) the long photocatalytic experiment shown in Fig. S18.

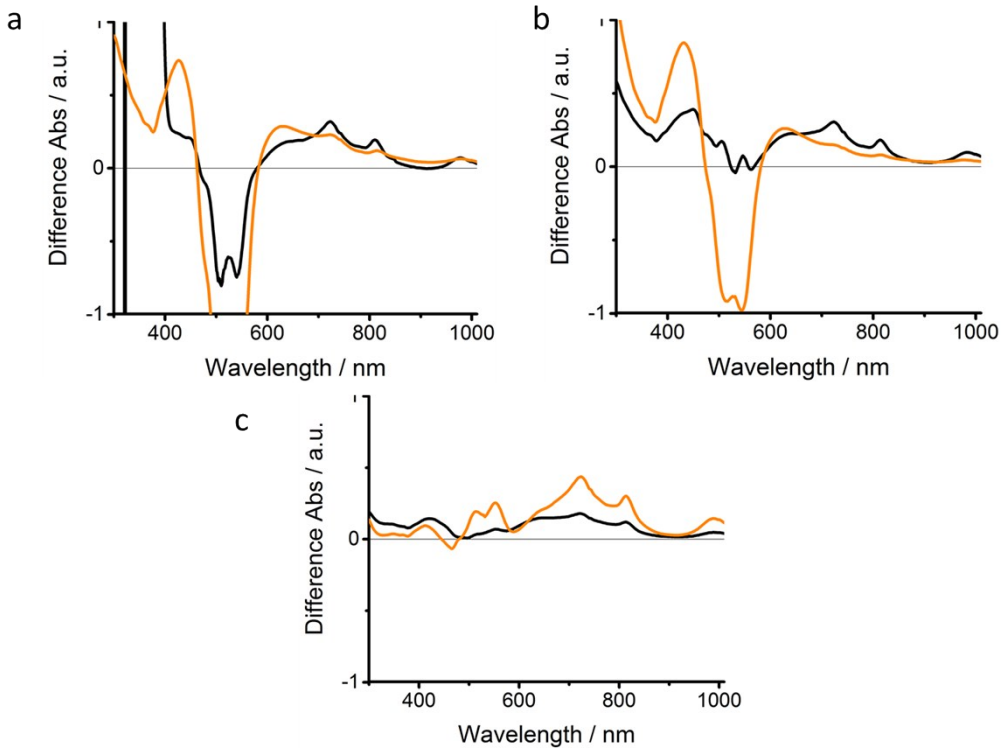

Figure S20. Difference absorption spectra of PBI-F (10 mg/mL) solutions in H_2O with 20 v/v% methanol with 1 mol% PVP-Pt NPs. Samples were irradiated with 470 nm (black lines) and 365 nm (orange lines) LEDs for one hour while solutions were housed in a sealed demountable 0.1 mm quartz cuvette. Three different pHs were measured; (a) pH 9.5 (b) pH 6 and (c) pH 4.5. For the pH 4.5 measurement, the heating from UV irradiation may have dissolved some aggregates which resulted in an increase in the absorbance between 400-600 nm. Visible hydrogen bubbles were also observed in this sample which may have affected the resulting spectrum. (a) is shown on the same y-axis scale as others to show clearly the difference in absorption between 600-900 nm which is of most importance.

λ / nm	E (= hυ/λ) x10^{-19} / mWcm^{-2}	Ratio of E_λ vs E_{365nm}	E irradiated onto sample / mWcm^{-2}
365	5.44	1	5
400	4.97	0.91	4.56
420	4.73	0.87	4.35
450	4.41	0.81	4.06
465	4.27	0.78	3.92
470	4.23	0.78	3.88
523	3.80	0.70	3.49
528	3.76	0.69	3.46
590	3.37	0.62	3.09
617	3.22	0.59	2.96
624	3.18	0.58	2.92

Figure S21. Calculation of normalised power outputs onto the sample from LEDs of various wavelengths, accounting for the number of photons supplied by each wavelength. Values used for the wavelength dependence hydrogen evolution study.

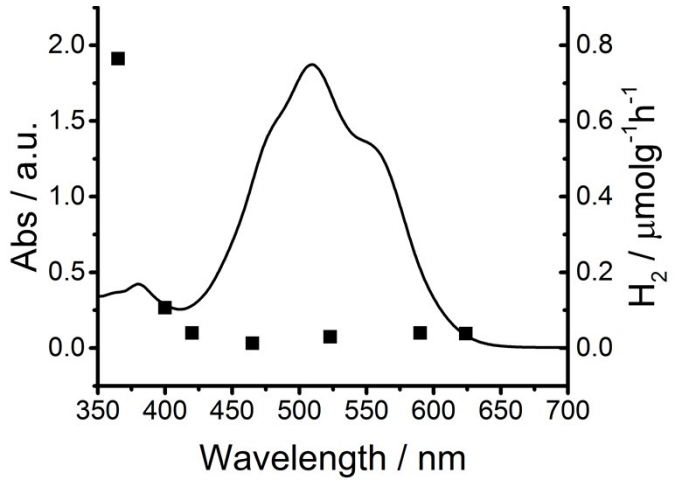

Figure S22. Wavelength dependence of hydrogen evolution (scatter) of a pH 4.5 solution of PBI-F (10 mg/mL), PVP-Pt NPs (1 mol%) with 20 v/v% methanol$_{(aq)}$. Overlaid is the UV-vis absorption spectrum of the solution without irradiation for reference (line).

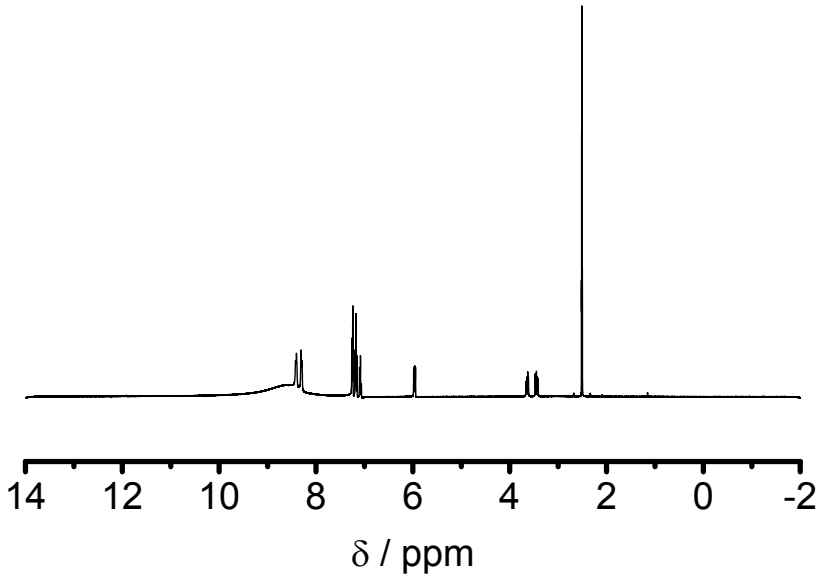

Figure S23. ^{1}H-NMR spectrum of PBI-F recorded in DMSO with a drop (*ca.* 5 μL) of TFA to aid solubility.

^{1}H NMR 400 MHz, (DMSO-d^{6}, 25 ˚C): δ (ppm) = 11.89 (s, 2H; -O<u>H</u>, CH(COO<u>H</u>)CH_2Phe); 8.15 (m, 8H, Perylene Core); 7.18 (m, 10H, -<u>Phe</u>); 5.97 (dd, 2H, J = 9.74, 5.62, C<u>H</u>(COOH)CH_2Phe); 4.51 (s, H_2O), 3.55 (m, C<u>H_2</u>-Phe), 2.50 (q, DMSO).

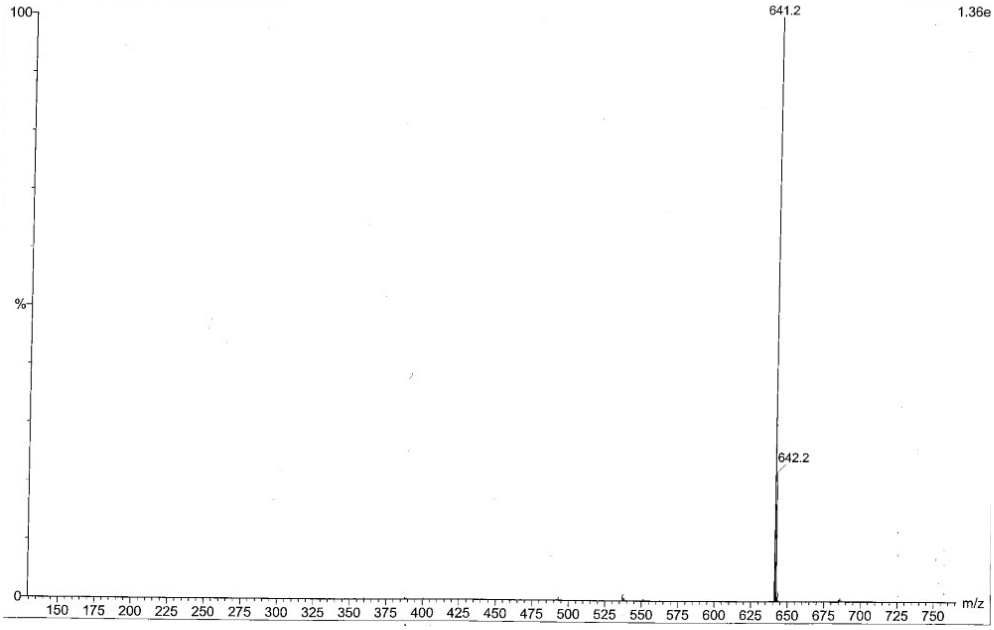

Figure S24. Mass Spectrum of PBI-F.

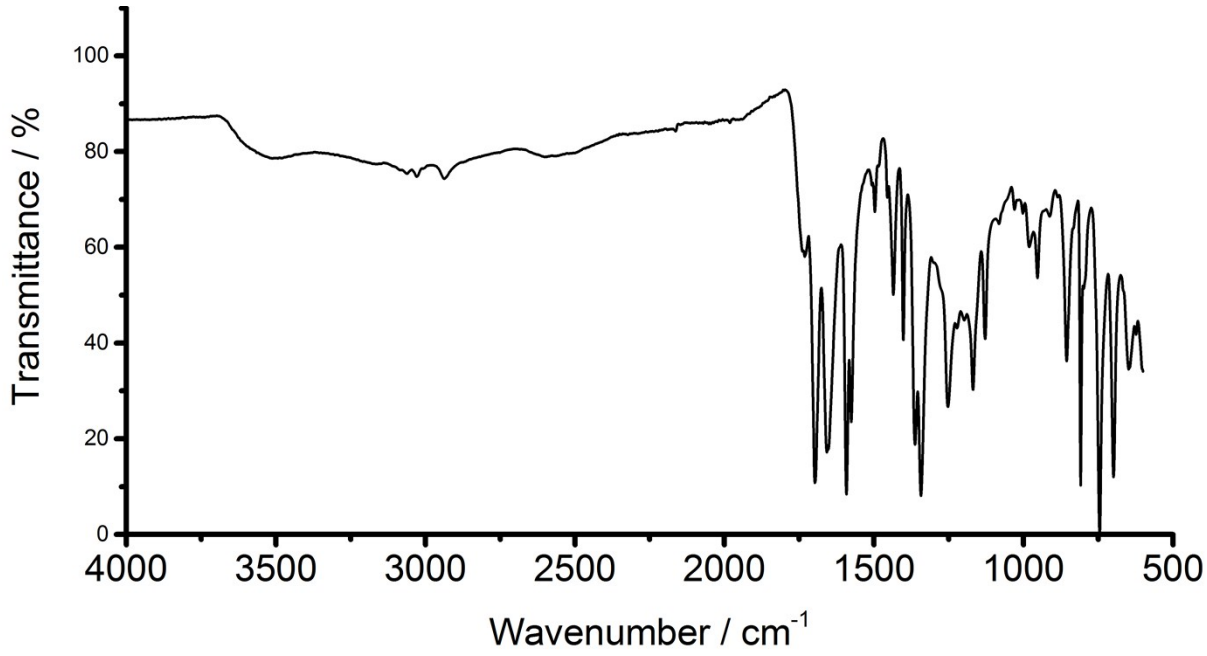

Figure S25. ATR FTIR spectrum of powdered PBI-F.

TON Calculation

(1) Moles of Pt in 5 mL sample: 4.8×10^{-4}
(2) Number of Pt atoms in 5 mL sample: 2.92×10^{20}
(3) Volume of Pt NPs with a 4 nm Pt core radius (measured via TEM): 267.95 nm^3
(4) Pt atom volume[9]: 0.0225 nm^3
(5) Number of Pt atoms in one NP [(3) / (4)]: 11909
(6) Number of Pt NPs in sample [((1) / (5)) * 6.022×10^{23} mol^{-1}) : 2.448×10^{16}
(7) Molecules of Hydrogen evolved in pH 4.5 sample after 307 hours (Experimental): 3.86×10^{18} mol
(8) TON per Pt atom ((2) / (7)): 1.32×10^{-2}
(9) TON per Pt NP ((6) / (7)): 158

References

1 A. Krężel and W. Bal, *J. Inorg. Biochem.*, 2004, **98**, 161–166.

2 www.sasview.org

3 N. M. Alexej Jerschow, *J. Magn. Reson.*, 1997, **375**, 372–375.

4 M. Liu, X. Mao, C. Ye, H. Huang, J. K. Nicholson and J. C. Lindon, *J. Magn. Reson.*, 1998, **132**, 125–29.

5 R. J. W. Lambert, I. Mytilinaios, L. Maitland and A. M. Brown, *Comput. Methods Programs Biomed.*, 2012, **107**, 155–163.

6 B. González, N. Calvar, E. Gómez and Á. Domínguez, *J. Chem. Thermodyn.*, 2007, **39**, 1578–1588.

7 V. J. Nebot, B. Escuder, J. F. Miravet, J. Smets and S. Fernández-Prieto, *Langmuir*, 2013, **29**, 9544–9550.

8 B. Escuder, M. LLusar and J. F. Miravet, *J. Org. Chem.*, 2006, **71**, 7747–7752.

9 A. Bondi, *J. Phys. Chem.*, 1964, **68**, 441–451.